CO_2 separation by a series of aqueous morpholinium-based ionic liquids with acetate anions

Ma, Chunyan; Shukla, Shashi Kant; Samikannu, Rakesh; Mikkola, Jyri-Pekka; Ji, Xiaoyan

Published in:
ACS Sustainable Chemistry and Engineering

DOI:
10.1021/acssuschemeng.9b05686

Published: 01/01/2020

Document Version
Accepted author manuscript

CO_2 separation by a series of aqueous morpholinium-based ionic liquids with acetate anions

Chunyan Ma[1,*], Shashi Kant Shukla[2], Rakesh Samikannu[2], Jyri-Pekka Mikkola[2,3], Xiaoyan Ji[1,*]

[1]Division of Energy Science/Energy Engineering, Department of Engineering Science and Mathematics, Luleå University of Technology, Luleå, 971 87, Sweden

[2]Technical Chemistry, Department of Chemistry, Chemical-Biological Centre, Umeå University, Umeå, 90871, Sweden

[3]Industrial Chemistry & Reaction Engineering, Johan Gadolin Process Chemistry Centre, Åbo Akademi University, Biskopsgatan 8, 20500, Finland

Abstract

In this work, CO_2 absorption capacities in a series of aqueous N-alkyl-N-methylmorpholinium-based ILs with acetate as counterpart anion were investigated. Amongst those ILs, N-butyl-N-methylmorpholinium acetate ([Bmmorp][OAc]) with the highest CO_2 absorption capacity was screened for thermodynamic modeling. The CH_4 absorption capacity in the aqueous [Bmmorp][OAc] was also measured in order to verify the results predicted from the thermodynamic modelling, and the comparison shows the reliability of the model prediction. After that, the aqueous [Bmmorp][OAc] solutions with 30 to 40 wt.% of water were selected to carry out process simulation for CO_2 separation from biogas, and it was found that using these aqueous [Bmmorp][OAc] gave rise to lower energy usage and smaller size of equipment than other physical solvents. The results suggest that aqueous [Bmmorp][OAc] solution can be used as an alternative to organic solvents and has the potential to decrease the cost of CO_2 separation.

Keywords: CO_2 separation, Ionic liquids, Thermodynamic modeling, Process simulation

1. Introduction

CO_2 separation plays an important role to mitigate CO_2 emissions due to burning of fossil fuels, and it is also of importance in biofuel production (e.g. biogas upgrading and bio-syngas purification and conditioning). The solvent-based absorption is the state-of-art technology for CO_2 separation, where various solvents, e.g. amine solutions, Selexol (i.e. dimethyl ethers of polyethylene glycol), and propylene carbonate, have been introduced.[1-3] However, the cost of these available technologies is too high, and the high volatility of these solvents leads to high solvent make-up rate and environmental problems. In addition, the high energy demand for solvent regeneration and the high corrosion rate to equipment of these solvents are also the problems needed to be overcome.[2] Therefore, the development of novel solvents with high CO_2 absorption capacity, low solvent degradation, low corrosion rate to equipment and low energy demand is essential.[4]

Ionic liquids (ILs) have gained a lot of attention as alternatives to volatile organic solvents for CO_2 separation because of their unique properties including the relatively high CO_2 absorption capacity, non-volatility, non-flammability, high thermal stability, tunability of structure and properties, and lower energy demand for solvent regeneration.[5, 6] Apart from offering the properties as conventional ILs, alkylmorpholinium based ILs possess lower toxicity than imidazolium, pyridinium or cyclic and acyclic ammonium ILs, leading to lower environmental effect.[7] Recently, the alkylmorpholinium based ILs have been investigated in many applications such as corrosion inhibitors, reaction media, catalysts, heat stabilizers, lubricants and cellulose dissolution.[7-9] However, the potential application of using these ILs in CO_2 separation has not been investigated.

On the other hand, the relatively high viscosity of ILs is the limitation of their practical applications, especially for CO_2 separation based on the traditional mass transfer units, e.g. the solvent-based absorption. Water as a green and cheapest solvent has been suggested as a co-solvent in the IL-based technologies to overcome the limitation of the high viscosity of ILs. Besides, water is also an unavoidable impurity in gas streams such as flue gas, biogas and bio-syngas, making it necessary to study the effect of water on the IL for CO_2 separation.

In this work, the CO_2 absorption capacities of N-allyl-N-methylmorpholinium acetates ([Ammorp][OAc]), N-ethyl-N-methylmorpholinium acetate ([Emmorp][OAc]), N-propyl-N-methyl-morpholinium acetate ([Pmmorp][OAc]) and N-butyl-N-methylmorpholinium acetate ([Bmmorp][OAc]) with water as co-solvent were investigated. Amongst those ILs, [Bmmorp][OAc] with the highest CO_2 absorption capacity was screened to study the effects of water content and temperature on the CO_2 absorption capacity and viscosity. In order to study the performances of the aqueous [Bmmorp][OAc] for CO_2 separation from biogas mainly containing CH_4 and CO_2 based on process simualtion, for pure [Bmmorp][OAc] with high viscosity, the COSMO-based method was used to estimate its propertires and the solubilities of CO_2 and CH_4. Combined with the measured CO_2 solubiliy, the thermodynamic modeling was carried out to represent the gas solubility (CO_2 and CH_4) in the aqueous IL solution with varied water content at different temperatures, and the CH_4 absorption capacity in aqueous [Bmmorp][OAc] was measured to verify the prediction from thermodynamic modeling. Finally, process simulation for CO_2 separation from biogas was carried out and its performance was compared with other physical solvents.

2. Experiment description

2.1. Materials

Most of the chemicals, such as *N*-methylmorpholine, allyl bromide, 1-bromobutane, bromoethane, 1-bromopropane were purchased from Sigma Aldrich Ltd. Alkyl-bromides were redistilled before further use. Acetic acid (100%) and potassium acetate (≥99.0%) were purchased from Merck. Amberlite IR-400 OH resin was purchased from Sigma Aldrich Ltd.

2.2. Preparation of ILs and aqueous ILs

Totally four kinds of alkylmorpholinium based ILs were investigated in this work as listed in Table 1. The synthesis of these four ILs was achieved in a two-step process as reported in our previous work.[7] Firstly, the *N*-alkyl-*N*-methylmorpholinium bromide was synthesized by a simple quaternization reaction of the alkyl-bromide and *N*-methylmorpholine. Subsequently, an ion exchange method was exploited for the conversion of bromide-based salt to highly pure acetate (99.99 %). The synthesized ILs were characterized by nuclear magnetic resonance (^{1}H- and ^{13}C-NMR) spectroscopy Bruker AV-

500 using deuterium oxide (D_2O) as the solvent, and the detail information can be found in the supporting material. The name, abbreviation, and structure of these ILs are shown in Table 1. High-quality deionized water was used to prepare the aqueous ILs in this work, and the exact water contents were determined with the WT-KF V100 Karl Fischer titrator.

Table 1 ILs investigated in this work

Name	Abbreviation	Structure
N-allyl-*N*-methylmorpholinium acetate	[Ammorp][OAc]	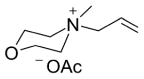
N-ethyl-*N*-methylmorpholinium acetate	[Emmorp][OAc]	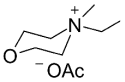
N-propyl-*N*-methylmorpholinium acetate	[Pmmorp][OAc]	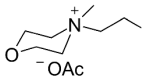
N-butyl-*N*-methylmorpholinium acetate	[Bmmorp][OAc]	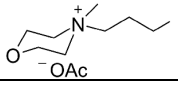

2.3. Gas absorption capacity measurement

The method to measure the gas absorption capacity is the same as that reported in our previous work.[10-12] Only a brief description was summarized here. The CO_2 (mole fraction ≥ 99.9%) and CH_4 (mole fraction ≥ 99.99%) used in this study were received from AGA AB (Linde group). As illustrated in Fig.1, the apparatus for measuring the gas absorption capacity consists of two main parts, which are the equilibrium cell with a magnetic stirrer (EC: 65.6 mL) and the gas reservoir (GR: 141.2 mL). Both the equilibrium cell and gas reservoir were placed in the water bath to keep the temperature stable during the experiment.

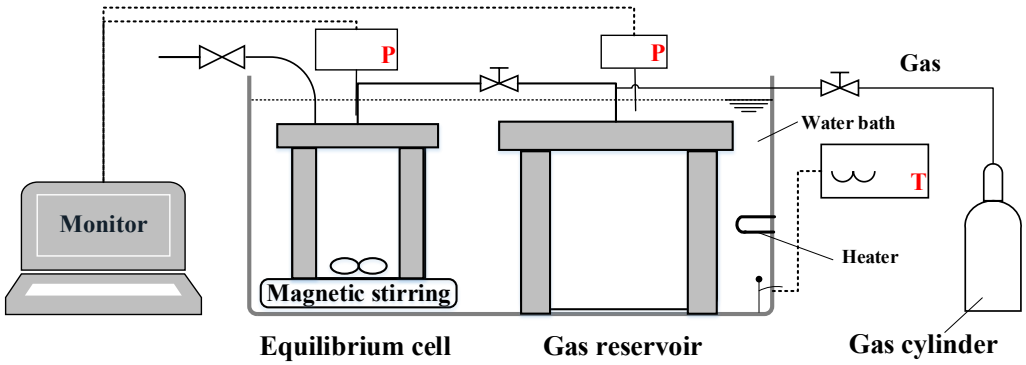

Fig. 1. Schematic diagram of the experimental apparatus

During the process, the pressures of the equilibrium cell and the gas reservoir were recorded by computer from the signal transferred by a pressure transducer. Once the pressures remained constant with the increase of time, it was considered to achieve the equilibrium state. All the measurements repeated at least twice. These pressures were used to calculate the amount of gas (*i*) dissolved in the precisely known amount of solvents as shown in Eq. (1).

$$n_i = \frac{P^{0,GR}V_{GR}}{Z_1RT} - \frac{P^{eq,GR}V_{GR}}{Z_2RT} - \frac{(P^{eq,EC} - P^s)(V_{EC} - V_L - V_r)}{Z_3RT} \quad \textbf{(1)}$$

where $P^{0,GR}$ is the initial pressure of the gas reservoir, $P^{eq,GR}$ and $P^{eq,EC}$ are the pressures of gas reservoir and equilibrium cell at equilibrium state, respectively, P^s is the saturated vapor pressure of the solvents at temperature T, Z_1, Z_2 and Z_3 are the compressibility factors of gas i corresponding to the pressures of $P^{0,GR}$, $P^{eq,GR}$ and ($P^{eq,EC}$ - P^s), V_{GR}, V_{EC} and V_r are denoted to the volumes of gas reservoir, equilibrium cell and magnetic rotor, respectively, V_L represents the volume of solvents, R is the gas constant, 8.314 $J \cdot mol^{-1} \cdot K^{-1}$, and T is the temperature in Kelvin. The values of Z_1, Z_2 and Z_3 were calculated from the second virial coefficients,[13] in which the gas phase was assumed as the pure component.

It should be mentioned that for the non-volatile ILs, their vapor pressure was negligible, and thus ILs were assumed to be non-existence in the vapor phase.[10, 11] Therefore, only gas (CO_2 or CH_4) and water were in vapor phase, and the vapor pressure of water was assumed to be the relation of the saturated vapor pressure of water and the concentration of water in liquid phase. The uncertainty of the gas solubility measurement consisted of the system errors including pressure, temperature, and the volumes of the absorber, buffer tank and pipeline. The uncertainties of pressure, temperature and volume from system errors were 0.002 MPa, 0.1 K and 0.5 mL, respectively. Based on all these above uncertainties, the overall uncertainty for the measured gas solubility was within ±1.5%.

The validity of our experimental method as well as the reliability of our reported data were confirmed by comparing the CO_2 solubility in ethylene glycol (at 303.2 K)[14] and water (at 308.2 K)[15, 16] from the data reported in literature with those obtained in this work (Fig. S5 in supporting material).

2.4. Viscosity measurement

The viscosity was measured using Bohlin CVO 100 rheometer in this work. The lower plate had a diameter of 60 mm. A cone-on-plate geometry was used with a 1° cone angle and 20 mm cone diameter. Before measuring the viscosity of ILs, the viscosity of glycerol was measured to confirm the validity and reliability of the measurement. The accuracy of temperature for the measurement was 0.1 K. The viscosity measurements were carried out at least twice and the average value was reported.

3. Results and discussion

3.1. Experimental results

3.1.1. The effect of cations on CO_2 absorption capacity

Considering that the viscosities of these pure ILs are very high, they cannot be used directly in the traditional mass transfer units, therefore, only aqueous ILs were studied. In this part, the CO_2 absorption capacities of four kinds of aqueous ILs (Table 1) with the same weight percentage (i.e. 40 wt.%) of water at pressures up to 2.0 MPa at 298.2 K were measured and compared. The method described in Section 2.3 was used to obtain the gas absorption capacity including mole fraction (x_{CO2})- and molality (m_{CO2})-based, and the results are shown in Table 2 and Fig. 2. It should be mentioned that the molality m_{CO2}, i.e. mole CO_2 per kg aqueous ILs solutions considering the molecular weight of the IL, was used for further discussion and comparison.

As we can see from Fig. 2, the CO_2 absorption capacity m_{CO2} for these aqueous ILs with different alkyl chains in the cations followed the order: [Bmmorp][OAc] > [Pmmorp][OAc] > [Ammorp][OAc] > [Emmorp][OAc], which indicates that the decrease of alkyl chain length in the cation leads to a decrease of gas capacity for the ILs with the same anion. In addition, the CO_2 absorption capacity of [Ammorp][OAc] was slightly lower than [Pmmorp][OAc] implying that the 'C=C' has a negative influence on the gas capacity but, not significantly. All these phenomena may prove that the structure of ILs has a great effect on the gas absorption capacity, even in the aqueous ILs.

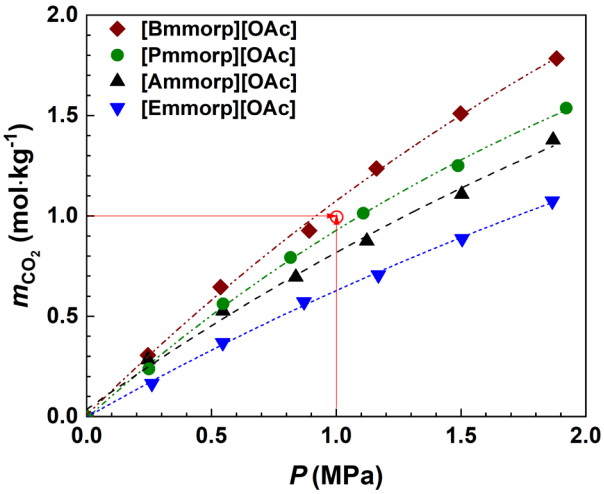

Fig. 2. CO_2 absorption capacity of these four IL-water binary systems with the same water content (40 wt.%). m_{CO2} is the molality of CO_2, mole CO_2 per kg aqueous ILs solutions. *P* is the pressure of CO_2. Lines: a guide for the eye

To further study the mechanism of CO_2 capture, the ^{13}C- and ^{1}H-NMR measurements of aqueous ILs before and after absorbing CO_2 were carried out. Specifically, the NMR measurement of aqueous ILs without contacting CO_2 was performed. After the test of CO_2 absorption at the pressure up to 2.0 MPa at 298.2 K, the equilibrium cell shown in Fig. 1 was opened, and the pressure was released to around atmospheric pressure. After that, the liquid was transferred to carry out the NMR measurements. The NMR spectra for the aqueous [Bmmorp][OAc] is depicted in Fig.3 as an example, and the similar results for the other ILs are included in the Supporting Material. The NMR spectral characteristics for the aqueous [Bmmorp][OAc] are shown as below:

[Bmmorp][OAc] before CO_2 absorption: ^{1}H-NMR (D_2O, 500Hz):- δ (ppm) 0.97 (m, 3H), 1.42 (m, 2H), 1.80 (m, 2H), 1.91 (s, 3H), 3.19 (s, 3H), 3.50 (m, 6H), 4.06 (s, 4H); ^{13}C-NMR (D_2O, 500Hz):- δ (ppm) 180.82, 65.18, 60.47, 59.60, 46.83, 23.56, 22.95, 19.16, 12.94

[Bmmorp][OAc] after CO_2 absorption: ^{1}H-NMR (D_2O, 500Hz):- δ (ppm) 0.97 (m, 3H), 1.42 (m, 2H), 1.80 (m, 2H), 1.91 (s, 3H), 3.19 (s, 3H), 3.50 (m, 6H), 4.05 (s, 4H); ^{13}C-NMR (D_2O, 500Hz):- δ (ppm) 180.72, 65.18, 60.47, 59.60, 46.84, 23.44, 22.95, 19.16, 12.92

The ^{13}C- and ^{1}H-NMR spectra showed that no new peaks were formed after absorbing CO_2, and the results meant that no new species were generated. Therefore, it can be concluded that for these aqueous ILs, the CO_2 absorption is physical absorption. Compared with the physical absorbents in literatures,[3] the m_{CO2} at 298.2 K and 1 MPa in the aqueous [Bmmorp][OAc] is higher than the typical value of the commercial physical absorbents, i.e. 1.0 mol·kg^{-1} (red dot in Fig. 2).[3]

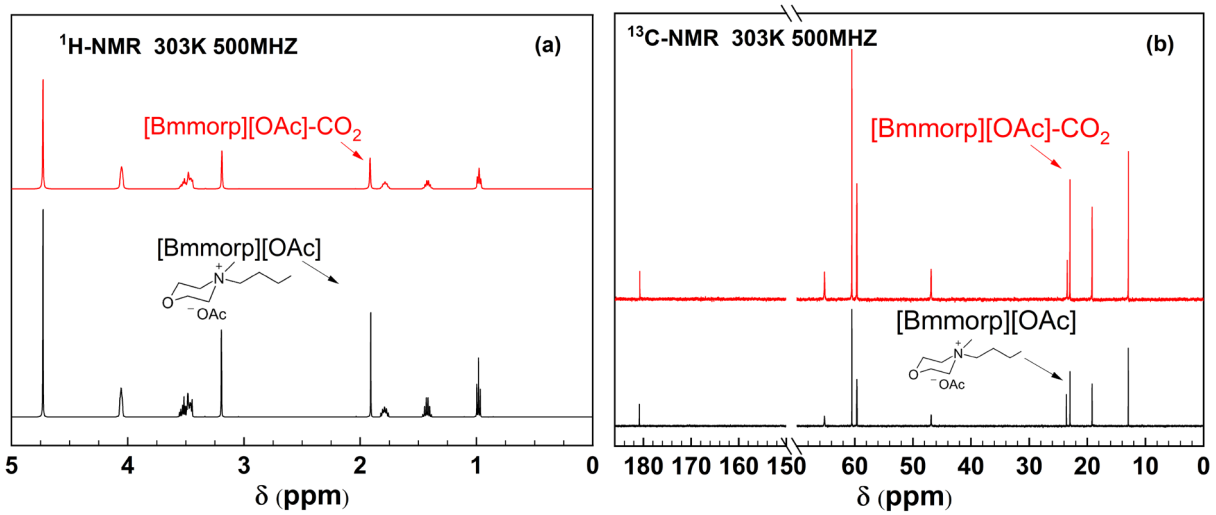

Fig. 3. ^{1}H (a) and ^{13}C NMR (b) spectra using D_2O as a solvent for aqueous ILs before and after absorbing CO_2. The values of δ are the chemical shift

3.1.2. The effects of water content and temperature on CO_2 absorption capacity

Based on the results in the Section 3.1, [Bmmorp][OAc] with the highest CO_2 absorption capacity was selected to further study the effects of water content and temperature on the CO_2 absorption capacity. Two water contents (20 and 40 wt.%) and three temperatures (298.2, 308.2 and 318.2 K) were studied in this part. The results are listed in Tables 2 and 3. Both the water content and temperature affected the CO_2 absorption capacity of aqueous [Bmmorp][OAc]. Specifically, the CO_2 absorption capacity decreased with the increases of temperature and water content. Moreover, the change of water content had a more significant influence on the CO_2 absorption capacity compared to the effect of temperature. When the water content decreased from 40 to 20 wt.%, the molality m_{CO2} at 1.0 MPa and 298.2 K increased around 2 times, i.e. m_{CO2} increased from 1.09 to 2.21 mol·kg^{-1}. For the solution with a water content of 20 wt.%, by increasing the temperature from 298.2 to 318.2 K, the values of m_{CO2} at 1.0 MPa decreased by 19.5%, showing that increasing temperature had a slightly negative influence on the CO_2

absorption capacity. This means that the temperature swing absorption/ desorption is unsuitable for this solvent.

Table 2 CO_2 absorption capacity in the mixture of IL-water with different water contents at 298.2 K

IL-H_2O	w_{H2O} [a] wt.%	P [b] MPa	x_{CO2} [c]	x_{H2O} [c]	x_{IL} [c]	n_{CO2}/n_{IL} [d] mol·mol^{-1}	m_{CO2} [e] mol·kg^{-1}
[Bmmorp][OAc]-H_2O	20	0.175	0.043	0.719	0.238	0.182	0.668
	20	0.423	0.089	0.684	0.227	0.393	1.446
	20	0.750	0.114	0.665	0.220	0.518	1.907
	20	1.100	0.138	0.648	0.215	0.643	2.365
	20	1.445	0.160	0.631	0.209	0.768	2.826
	20	1.865	0.185	0.612	0.203	0.913	3.359
	40	0.245	0.012	0.879	0.109	0.111	0.306
	40	0.536	0.025	0.867	0.108	0.234	0.646
	40	0.891	0.036	0.858	0.107	0.336	0.927
	40	1.161	0.047	0.848	0.105	0.448	1.236
	40	1.498	0.057	0.839	0.104	0.547	1.510
	40	1.883	0.067	0.830	0.103	0.646	1.784
[Ammorp][OAc]-H_2O	40	0.245	0.011	0.872	0.117	0.095	0.284
	40	0.546	0.020	0.864	0.116	0.170	0.508
	40	0.837	0.026	0.858	0.115	0.229	0.683
	40	1.122	0.033	0.853	0.114	0.287	0.857
	40	1.503	0.040	0.846	0.113	0.357	1.063
	40	1.875	0.055	0.833	0.112	0.491	1.463
[Pmmorp][OAc]-H_2O	40	0.249	0.009	0.874	0.116	0.081	0.238
	40	0.546	0.022	0.863	0.115	0.190	0.562
	40	0.817	0.030	0.856	0.114	0.268	0.792
	40	1.108	0.039	0.849	0.113	0.343	1.013
	40	1.488	0.047	0.841	0.112	0.424	1.250
	40	1.922	0.058	0.832	0.111	0.521	1.537
[Emmorp][OAc]-H_2O	40	0.261	0.006	0.869	0.124	0.052	0.165
	40	0.545	0.014	0.863	0.123	0.116	0.368
	40	0.870	0.022	0.856	0.122	0.180	0.571
	40	1.168	0.027	0.851	0.121	0.223	0.705
	40	1.504	0.034	0.846	0.119	0.283	0.886
	40	1.866	0.041	0.840	0.117	0.347	1.074

[a] w_{H2O} is the weight percentage of water. [b] P is the pressure. [c] x_i is the mole fraction of component i. [e] n_{CO2}/n_{IL} is the absorption capacity of IL in aqueous ILs, mole CO_2 per mol IL. [d] m_{CO2} is the molality of CO_2, mole CO_2 per kg aqueous ILs solutions.

Table 3 CO_2 absorption capacity in [Bmmorp][OAc] with 20 wt.% water at different temperatures

298.2 K			**308.2 K**			**318.2 K**		
P MPa	x_{CO2}	m_{CO2} mol·kg^{-1}	P MPa	x_{CO2}	m_{CO2} mol·kg^{-1}	P MPa	x_{CO2}	m_{CO2} mol·kg^{-1}
0.175	0.043	0.668	0.173	0.043	0.670	0.184	0.040	0.619
0.423	0.089	1.446	0.444	0.082	1.322	0.453	0.073	1.159
0.750	0.114	1.907	0.769	0.106	1.763	0.780	0.097	1.584
1.100	0.138	2.365	1.090	0.124	2.102	1.186	0.119	1.992
1.445	0.160	2.826	1.447	0.146	2.527	1.535	0.133	2.278
1.865	0.185	3.359	1.881	0.167	2.963	1.936	0.151	2.639

3.1.3. The CH_4 absorption capacity in aqueous [Bmmorp][OAc]

The CH_4 absorption capacities of aqueous [Bmmorp][OAc] with 23 wt.% of water at pressures up to 2.0 MPa at 298.2 K were measured. The results are shown in Table 4. Compared to the results listed in Table 4 and those listed in Table 3, this aqueous IL has very low solubility to CH_4. The CH_4 absorption capacity at 1.0 MPa and 298.2 K was around 0.13 $mol \cdot kg^{-1}$, which was only 6% of CO_2 absorption capacity at the same condition. This result indicated high selectivity of CO_2 over CH_4 of aqueous [Bmmorp][OAc].

Table 4 CH_4 absorption capacity in [Bmmorp][OAc] with 23 wt.% water at 298.2 K

IL-H_2O	w_{H2O} wt.%	*P* MPa	x_{CH4}	x_{H2O}	x_{IL}	n_{CH4}/n_{IL} $mol \cdot mol^{-1}$	m_{CH4} $mol \cdot kg^{-1}$
[Bmmorp][OAc]-H_2O	23	0.1535	0.0011	0.782	0.217	0.005	0.017
	23	0.3495	0.0030	0.781	0.216	0.014	0.049
	23	0.5975	0.0049	0.779	0.216	0.023	0.081
	23	0.9195	0.0075	0.777	0.215	0.035	0.124
	23	1.3095	0.0105	0.775	0.215	0.049	0.173
	23	1.6345	0.0120	0.774	0.214	0.056	0.199
	23	2.0015	0.0139	0.772	0.214	0.065	0.230

3.1.3. The effect of water content and temperature on viscosity

Viscosity is an important factor directly related to the mass-transfer rate. Therefore, the viscosity of [Bmmorp][OAc] with different water contents was measured, at temperatures of 298.2, 308.2 and 318.2 K (Fig. 4). As we can see from Fig. 4, the viscosity decreased dramatically with the increase of the water content. Specifically, the viscosity decreased from 570 to 50 mPa s when the water content increased from 3.6 to 23 wt.%. When the water content was higher than 35 wt.%, the viscosity of solvent was lower than 10 mPa s, making it possible to be used in the traditional mass-ransfer units. In addition, the increase in temperature led to a decrease of viscosity.

According to the results in section 3.1.2, the aqueous [Bmmorp][OAc] solutions with around 20 wt.% of water showed high CO_2 absorption capacity (>2.2 $mol \cdot kg^{-1}$ at 1 MPa and 298.2 K), indicating the great potential in CO_2 separation. It has been reported that the viscosity of ILs may greatly increase after absorbing CO_2 especially for the solvent with relatively high absorption capacity. Therefore, the aqueous [Bmmorp][OAc] with around 20 wt.% of water was selected to investigate its viscosity before

and after the absorption of CO_2 at the temperatures of 298.2, 308.2 and 318.2 K. The results are depicted in Fig. 5.

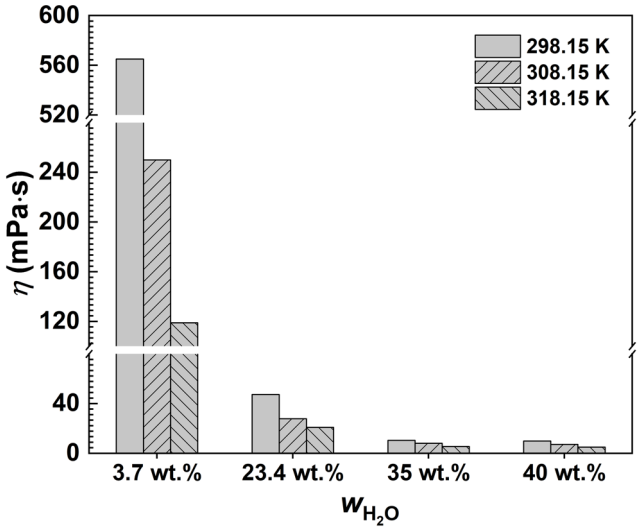

Fig. 4. The viscosity of [Bmmorp][OAc] with different water contents at different temperatures, i.e. 298.2, 308.2 and 318.2 K.

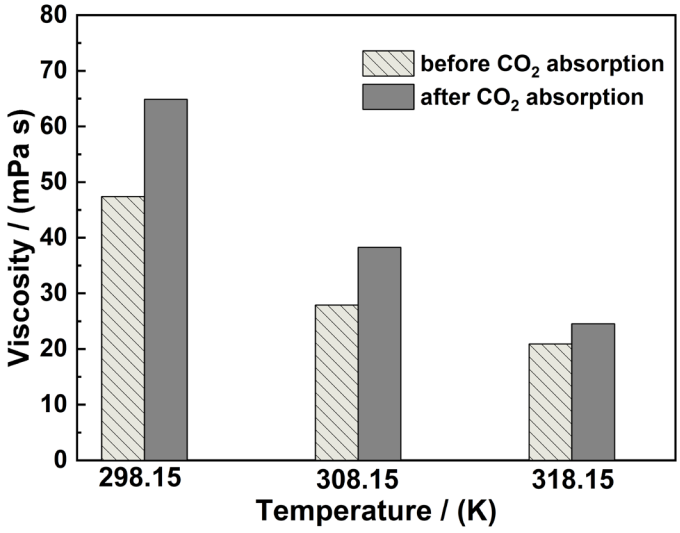

Fig. 5. The viscosity of [Bmmorp][OAc] with water content of around 23.4 wt.% before and after the absorption of CO_2 at different temperatures

As we can see from Fig. 5, after absorbing CO_2, the viscosity of aqueous [Bmmorp][OAc] solutions increased, and the difference of the viscosity before and after absorbing CO_2 decreased with the increase of temperature. However, even at 318.2 K, the viscosity of aqueous [Bmmorp][OAc] with 23.4 wt.% water (21 mPa·s) was still too high to apply in a traditional mass transfer unit. Therefore, the solution with water content lower than 25 wt.% should not be considered. Meanwhile, the water content should

not be higher than 40 wt.% (CO_2 absorption capacity ≈1.09 mol·kg^{-1} at 1 MPa and 298.2 K) in order to compete with commercial organic solvents.

3.2. COSMOthermX calculation for pure [Bmmorp][OAc]

For the studied pure IL, the viscosity was too high, and it was difficult to measure the gas absorption capacities reliably. Meanwhile, such high viscous IL cannot be used directly in the conventional mass-ransfer units. Therefore, in this work, the properties of pure IL and the corresponding gas solubility were estimated theoretically.

The COSMO-RS theory[17, 18] based methods show a very promising and priori predictive power for various properties of IL solutions because no adjustable parameters are needed making it readily applicable to all types of IL solutions.[19-21] In this work, the [C+A] model treating the ILs as equimolar mixtures of cations and anions, i.e. with an independent cation and anion, was used to define the structure of the IL. The geometry of all compounds was optimized at the B3LYP/6-31++G** computational level using the software Turbomole7.3[22], which was also used to produce the COSMO files. After that, the software COSMOthermX (version C30, Release 18.0)[23, 24] using the COSMO files as an input was used to estimate the gas absorption capacity and the thermophysical properties. The estimated results of mass density, viscosity, electrical conductivity and heat capacity for the pure [Bmmorp][OAc] are shown in Table S1, and the predicted gas absorption capacities (i.e. CO_2 and CH_4) in pure [Bmmorp][OAc] are shown in Fig. 6. As we can see from Fig.6, the CO_2 and CH_4 absorption capacities were around 2.15 and 0.095 mol kg^{-1} at 1 MPa and 298.15 K, respectively, and with the increase of temperature, the gas absorption capacity decreased.

The enthalpy of solution $\Delta_{sol}H$ is related to the strength of interaction between the liquid and the gas. Here, the $\Delta_{sol}H$ was obtained using the following equation[25]:

$$\frac{\Delta_{sol}H}{R} = \left(\frac{\partial \ln P_i}{\partial (1/T)} \right)_{x_i} \quad \textbf{(2)}$$

As we can see from Table 5, the negative values of $\Delta_{sol}H$ showed the strong intermolecular bonding between the gas (CO_2 and CH_4) and IL. It also showed that the process of CO_2 and CH_4 absorption in [Bmmorp][OAc] was exothermic in nature. As we can see from Table 5, the absolute $\Delta_{sol}H$ value of

CO_2 was around 19 kJ mol^{-1}, which was twice of that of CH_4 (about 9 kJ mol^{-1}). This result meant the interaction of CO_2 and IL was much stronger than that of CH_4 and IL.

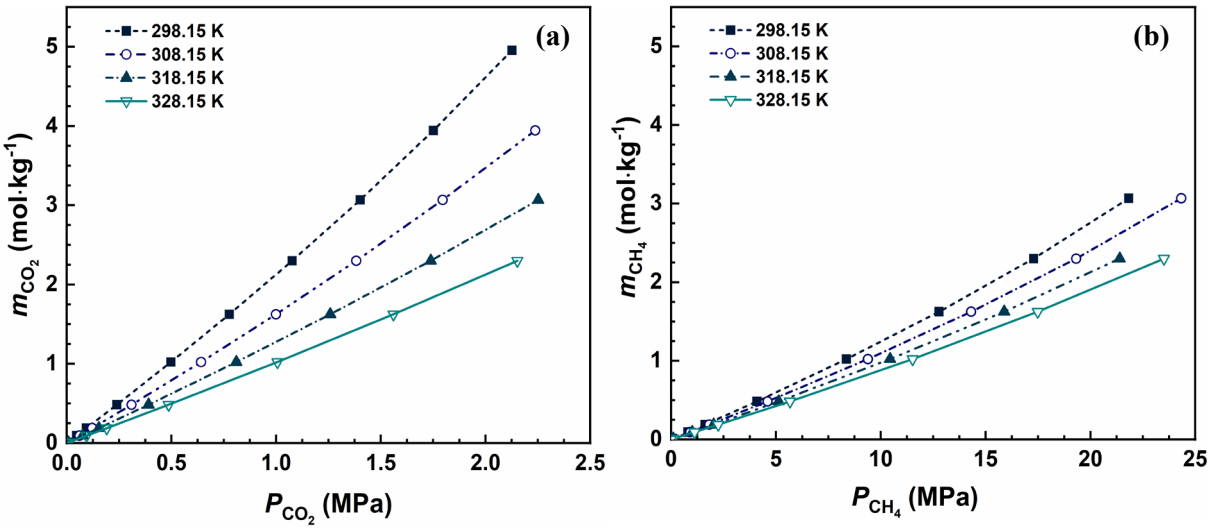

Fig. 6. CO_2 (a) and CH_4 absorption capacity (b) based on molality for [Bmmorp][OAc] from 298.15 to 328.15 K estimated by COSMOthermX

Table 5 Enthalpy of solution $\Delta_{sol}H$ of CO_2 and CH_4 in [Bmmorp][OAc]

x_{CO2}	$\Delta_{sol}H$ / (kJ mol^{-1})	x_{CH4}	$\Delta_{sol}H$ / (kJ mol^{-1})
0.333	-18.8	0.333	-8.3
0.261	-18.9	0.261	-8.5
0.182	-19.1	0.182	-8.7
0.095	-19.2	0.095	-8.9
0.039	-19.3	0.039	-9.0
0.002	-19.4	0.002	-9.1

3.3. Thermodynamic modeling

Based on the data from the experiment and theoretical prediction in Section 3.2, thermodynamic modeling was carried out. Firstly, the critical properties (T_C, P_C, and V_C), normal boiling temperature (T_b) and acentric factor (w) were estimated by the group contribution method (Table 6).[26, 27]

Table 6 Properties of [Bmmorp][OAc] estimated by the group contribution method[26, 27]

Property	T_b / (K)	T_C / (K)	P_C / (MPa)	V_C / (m^3 kmol^{-1})	M / (g mol^{-1})	w
[Bmmorp][OAc]	477.4	615.1	2.1	0.7162	217.306	0.966

Due to the negligible vapor pressure of the IL, it was assumed that [Bmmorp][OAc] only existed in the liquid phase. For water, the extended Raoult's law was used to represent the vapor-liquid equilibrium:

$$Py_w\varphi_w^v = x_w\gamma_w P_w^s \quad \textbf{(3)}$$

where P is the system pressure, y is the mole fraction in the vapor phase, φ^v is the fugacity coefficient in the vapor phase, x is the mole fraction in the liquid phase, γ is the activity coefficient in the liquid phase, P^s is the vapor pressure of the pure solvent at particular temperature, and the subscript w refers to water.

The solubility of gas (i) in a solvent follows the Henry's law and can be expressed as:

$$Py_i\varphi_i^v = H_i\left(T,P\right)x_i\gamma_i / \gamma_i^\infty \quad \textbf{(4)}$$

where $H_i(T, P)$ is the Henry's constant of gas i in the solvent at the temperature T and pressure P, γ^∞ is the activity coefficient at infinite dilution in the liquid phase.

The Henry's constant for gas i in the pure solvent j was calculated by the following equations:

$$H_{ij}\left(T,P\right) = H_{ij}\left(T\right)\exp\left(\frac{V_{ij}^\infty P}{RT}\right) \quad \textbf{(5)}$$

$$\ln H_{ij}(T) = A_{ij} + B_{ij}/T + C_{ij}\ln T + D_{ij}T \quad \textbf{(6)}$$

where $H_{ij}(T, P)$ is the Henry's constant of gas i in the pure solvent j at the system temperature and pressure, $H_{ij}(T)$ is the Henry's constant of gas i in the pure solvent j at zero pressure, V_{ij}^∞ is the infinite dilution partial volume of gas i in the pure solvent j calculated from the Brelvi-O'Connell model [28] with the characteristic volumes for the gas i (V_i^{BO}) and solvent j (V_j^{BO}), respectively. The general form of the Brelvi-O'Connell model is:

$$V_{ij}^\infty = fcn\left(V_i^{BO}, V_j^{BO}, V_j^l\right) = v_1 + v_2 \times T \quad \textbf{(7)}$$

where V_j^l is the liquid molar volume of solvent j.

The Henry's constant of gas i in the mixed solvent ($H_{i,\,mix}$) was calculated from those in the pure solvents [29]:

$$\ln\left(\frac{H_{i,mix}}{\gamma^{\infty}_{i,mix}}\right)=\sum_j w_j \ln\left(\frac{H_{ij}(T,P)}{\gamma^{\infty}_{ij}}\right)$$
$$w_j=\frac{x_j\left(V_{cj}\right)^{2/3}}{\sum_k x_k\left(V_{ck}\right)^{2/3}} \quad (8)$$

where $\gamma^{\infty}_{i,mix}$ is the activity coefficient of gas i at infinite dilution in the mixed solvent, $\gamma^{\infty}_{i,j}$ is the activity coefficient of gas i at infinite dilution in the pure solvent j, and w_j is the weighting factor. V_{cj} was set to be the critical volume of the solvent j.

The Redlich-Kwong (RK) equation of state was used to calculate φ_i^v for the gaseous components with the parameters taken from Aspen databank directly.[30] The Non-Random Two-Liquid (NRTL) model was used to calculate the activity coefficient γ in the liquid phase by the following equation:

$$\ln\gamma_i=\frac{\sum_{j=1}^{m}\tau_{ji}G_{ji}x_j}{\sum_{l=1}^{m}G_{li}x_l}+\sum_{j=1}^{m}\frac{G_{ij}x_j}{\sum_{l=1}^{m}G_{lj}x_l}\left[\tau_{ij}-\frac{\sum_{r=1}^{m}x_r\tau_{rj}G_{rj}}{\sum_{l=1}^{m}G_{lj}x_l}\right]$$
$$G_{ij}=\exp\left(-c_{ij}\tau_{ij}\right),\ G_{ji}=\exp\left(-c_{ji}\tau_{ji}\right) \quad (9)$$
$$\tau_{ij}=a_{ij}+b_{ij}/T,\ \tau_{ji}=a_{ji}+b_{ji}/T,\ c_{ij}=c_{ji}(i\neq j)$$

where m is the number of components, τ_{ij} is the NRTL binary interaction energy parameter, and c_{ij} is the non-randomness factor and it was fixed to be 0.2 in this work.

In modeling, for CO_2-H_2O, the parameters in Eq. (6) to calculate Henry's constant and in Eq. (9) to calculate NRTL binary parameters were directly taken from the Aspen databank as listed in Tables 7 and 9, respectively. For CH_4-H_2O, the parameters in Eq. (6) to calculate Henry's constant were directly taken from the Aspen databank, while the parameters in Eqs. (7) and (9) were obtained from the fitting of the experimental data. The predicted solubilities at low pressures (i.e. under 1 MPa) and different temperatures from COSMOthermX in Section 3.2 were used to obtain the parameters in Eq. (6) by setting the NRTL binary interaction parameters to be zero and neglecting the effect of pressure. While based on the predicted solubilities at relatively high pressures (i.e. above 1 MPa), from COSMOthermX, V_{ij}^{∞} in Eq. (7), was set to be the adjustable parameters to describe the gas solubility at relatively high pressures.

To model the gas solubility in [Bmmorp][OAc] with water as co-solvent, based on the parameters obtained from the gas solubility in the pure solvent with Eqs. (5)-(7), the Henry's constant of gas *i* in the aqueous [Bmmorp][OAc] was calculated according to Eqs. (8) and (9), where the NRTL binary parameters (τ_{ij}) in Eq. (9) between [Bmmorp][OAc] and H_2O were set to be the adjustable parameters and fitted to the experimental data of the CO_2 solubility in the aqueous [Bmmorp][OAc] reported in Section 3.1.2. Obviously, the model results agreed well with the experimental data as we can see from Fig. 7 with an average relative deviation (ARD) of 8.78%. All the parameters in Tables 7, 8 and 9 were implemented into Aspen Plus.

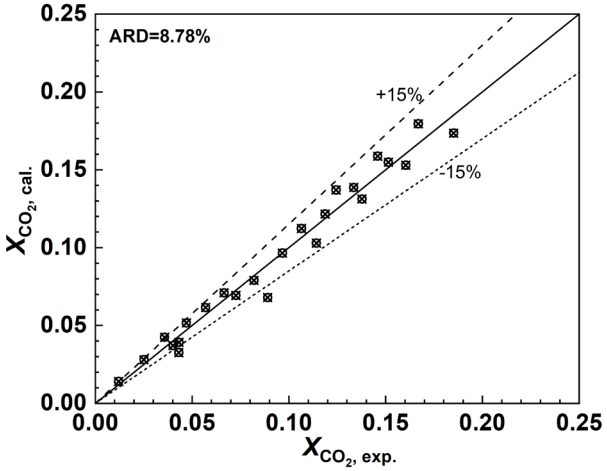

Fig. 7 Parity plot for [Bmmorp][OAc]-H_2O-CO_2 system, x_{CO2}: experiment vs. model.

Based on the parameters obtained from thermodynamic modeling (listed in Tables 7, 8 and 9), the solubilities of CH_4 was predicted and shown in **Fig. 8a**. The predicted CH_4 solubility was compared with the measured CH_4 solubility listed in Table 4 for verification. The results showed that model results agreed with the experimental data very well (**Fig. 8a**).

In order to study the water effect on the gas solubility, based on these parameters the solubility of CH_4 and CO_2 as well as the selectivity of CO_2 over CH_4 ($S_{CH4/CO2}$) for the gas mixture (50 mol.% CH_4, 50 mol.% CO_2) in the aqueous [Bmmorp][OAc], with different water amounst under the operating conditions of 298.2 K and 0.8 MPa, were predicted as shown in **Fig. 8b**. Here, the selectivity $S_{CH4/CO2}$ was calculated by Eq. (10):

$$S_{CH_4/CO_2} = \frac{y_{CH_4} / x_{CH_4,j}}{y_{CO_2} / x_{CO_2,j}} \quad \textbf{(10)}$$

where y_{CH4} and y_{CO2} are the mole fraction of CH_4 and CO_2 in gas phase, respectively, $x_{CH4,j}$ and $x_{CO2,j}$ are the more fraction of CH_4 and CO_2 in solvent *j*.

As we can see from **Fig. 8b**, the CO_2 absorption capacity based on molality decreased dramatically with the increase of water content. The selectivity increased gradually with the increase of water content, which meant that water had a positive effect on the selectivity of this IL solution. Since both solubility and selectivity influence the performance of the solution in the gas separation process, it is necessary to study its performance by process simulation.

Table 7 Parameters for calculating the Henry's Constant $H_{i,j}(T)$ in Eq. (6) (in MPa)

Solute *i*	Solvent *j*	A_{ij}	B_{ji}	C_{ij}	D_{ji}
CO_2	*H_2O	156.897	-8477.71	-21.9574	0.005781
CH_4	*H_2O	181.478	-9111.67	-25.0379	0.000143
CO_2	[Bmmorp][OAc]	8.2302	-2184.8	0	0
CH_4	[Bmmorp][OAc]	7.3482	-1087.1	0	0

*From Aspen Databank

Table 8 The parameters for estimating V_{ij}^{∞} in Eq. (7)

i-j	CO_2-H_2O	CO_2-[Bmmorp][OAc]	CH_4-H_2O	CH_4-[Bmmorp][OAc]
v_1	28.612	2637.964	44.419	1677.762
v_2	-0.00598	-7.261	-0.0243	-4.108

Table 9 The NRTL binary interaction parameters in Eq. (9)

Component *i*	Component *j*	a_{ij}	a_{ji}	b_{ij}	b_{ji}	$c_{ij}= c_{ji}$
CO_2	*H_2O	10.064	10.064	-3268.14	-3268.14	0.2
CH_4	H_2O	11.024	11.024	-3554.37	-3554.37	0.2
CO_2	[Bmmorp][OAc]	0	0	0	0	0.2
CH_4	[Bmmorp][OAc]	0	0	0	0	0.2
H_2O	[Bmmorp][OAc]	126.474	-25.418	-37303.09	7338.70	0.2

*From Aspen Databank

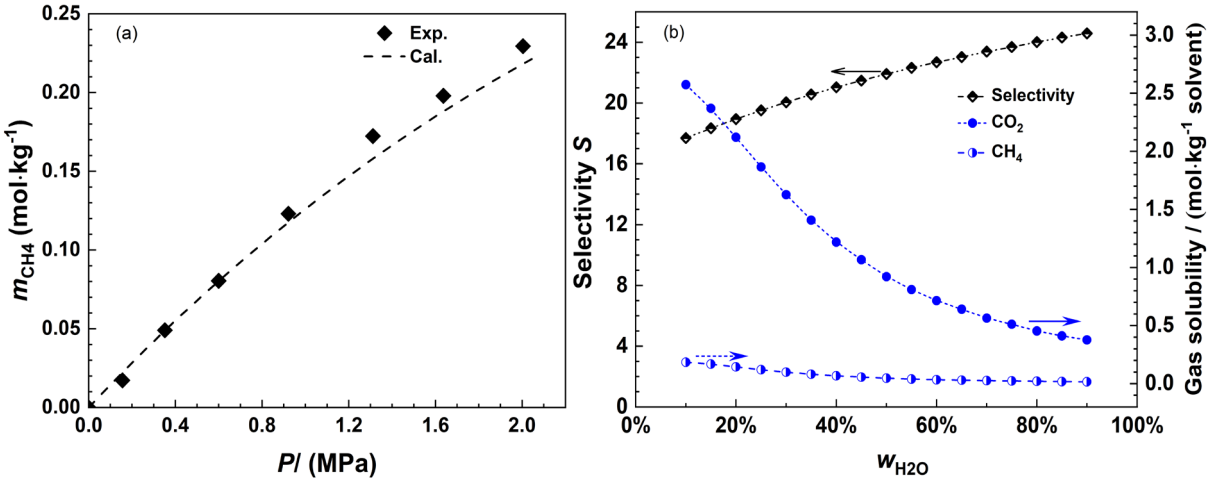

Fig. 8. (a) CH_4 solubility of 23 wt.% H_2O in [Bmmorp][OAc]: model vs. experiment; (b) water effect on gas solubility and selectivity of CO_2 over CH_4 for aqueous [Bmmorp][OAc] at 298.2 K.

3.4. Process simulation and comparison

The parameters obtained from section 3.3 were embedded into Aspen Plus v.10 to carry out process simulation based on the process shown in **Fig. 9**. Considering the high viscosity of the aqueous [Bmmorp][OAc] with less than 25 wt.% water and low CO_2 absorption capacity (less than 1 mol·kg^{-1} solvent) of the aqueous [Bmmorp][OAc] with higher than 40 wt.% water, the performances of CO_2 separation from biogas using the solutions with 30 to 40 wt.% water in [Bmmorp][OAc] were investigated. The detail information about the process of CO_2 separation from biogas can be found in our previous work[3, 30]. In this work, the raw biogas was set to be a mixture of 65 mol.% CH_4 and 35 mol.% CO_2 with a plant capacity of 250 Nm^3 h^{-1} and the temperature for biogas upgrading was set to be 293.2 K. The CO_2 removal efficiency and the CH_4 loss were set to be the same as those in our previous work[3], i.e. 96.2% and 0.5%--, respectively.

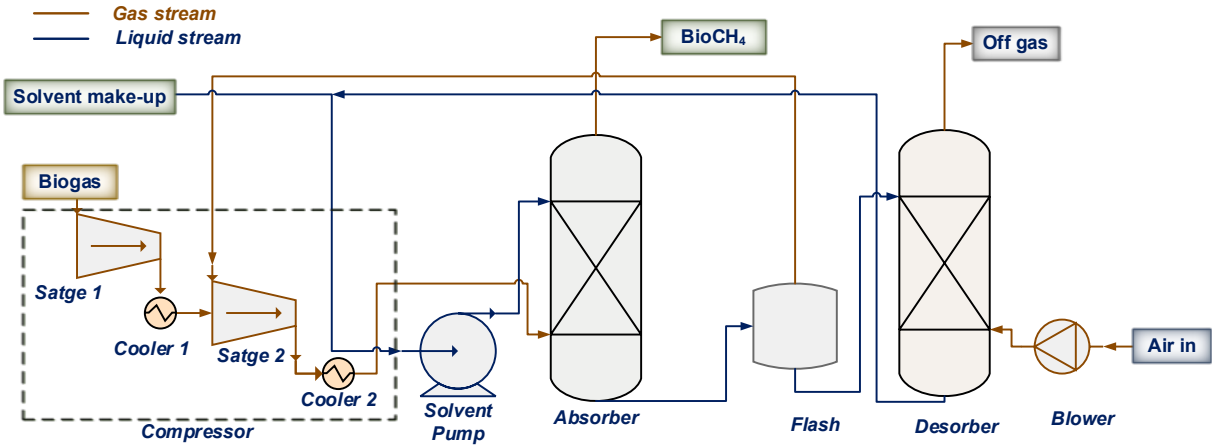

Fig. 9. Conceptual process of CO_2 separation from biogas

In this work, the energy usage consists of the parts from the biogas compressors, solvent pump, gas blower in desorption step as well as the other contributions including heat duty of coolers as we can see from **Fig. 9**. For the sharp increase in temperature during the biogas compression, the coolers were used to cool compressed biogas. For a better comparison, the overall energy usage was expressed by the equivalent energy penalty from both electrical power and thermal energy. The electricity required by compressors, gas blower, solvent pump in the biogas upgrading process conversed to the thermal energy of steam. The conversion efficiency of steam to electricity was set to be 0.3. In addition, the energy efficiency of this biogas upgrading process was also calculated by the following Eq. (11)

$$EF = \frac{Q_{out,biomethane}}{Q_{in,biogas} + Q_{input}} \quad \textbf{(11)}$$

where $Q_{\text{in, biogas}}$ and $Q_{\text{out, biomethane}}$ represent the lower heat values (LHV) of biogas and biomethane, respectively, Q_{input} represents the energy usage in biogas upgrading process. The LHV of CH_4 was 50.01 $MJ \cdot kg^{-1}$.

The total energy usage, energy efficiency as well as the diameters of absorber and desorber for the process using aqueous [Bmmorp][OAc] were compared with those for the process with the commercial solvents, i.e. water, dimethyl ethers of polyethylene glycol (DEPG), propylene carbonate (PC). The results are shown in **Fig. 10**.

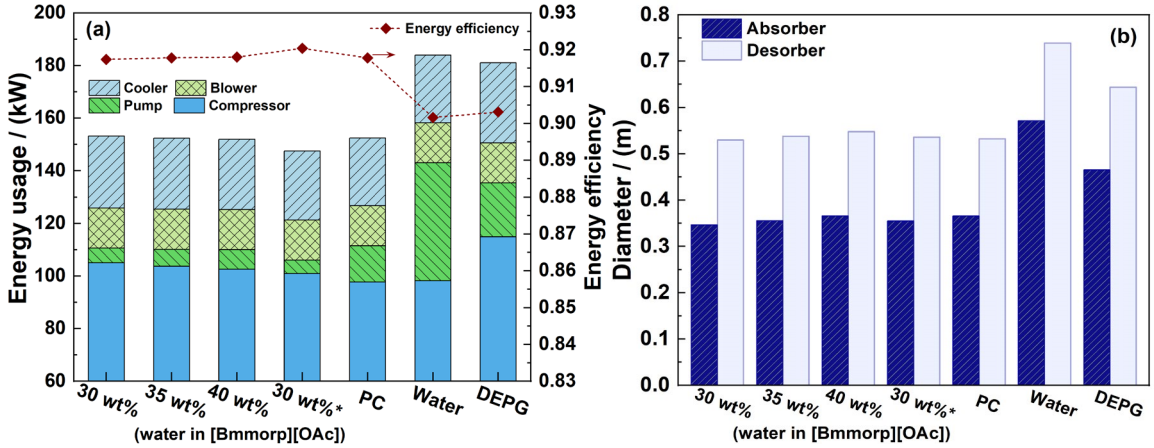

Fig. 10. Energy usage and energy efficiency (a) as well as diameters of the absorber/desorbed (b) for different solvents

As we can see from **Fig. 10a**, for all the solvents the energy efficiency was higher than 90%, and the energy efficiency increased with the decrease in energy usage. The energy usage of aqueous [Bmmorp][OAc] and PC as solvents was much lower than those of DEPG and water. With the increase of water amount from 30 to 40 wt.% in [Bmmorp][OAc], energy usage decreased slightly, which was slightly lower than that of PC. The main reason for the low energy usage was that using aqueous [Bmmorp][OAc] significantly decreased the energy usage from the solvent pump as we can see obviously from **Fig. 10a**. However, the energy usage from the compressor was still high but decreased with the increase of water amount of aqueous [Bmmorp][OAc], which was related to the selectivity of the solvent. On the other hand, the dimeters for the aqueous [Bmmorp][OAc] increased with the increase of water amount as we can see from **Fig. 10b**.

Considering energy usage and sizes of equipment, the aqueous [Bmmorp][OAc] with 30 wt.% of water is a better option. As we can see from **Fig.10b**, compared with other commercial solvents, the diameter of absorber using 30 wt.% water in [Bmmorp][OAc] was 5%, 26% and 39% smaller than those using PC, DEPG and water, respectively. While the diameter of the desorber using 30 wt.% water T [Bmmorp][OAc] was 1%, 18% and 28% smaller than those using PC, DEPG and water, respectively. This, in essence, means that choosing 30 wt.% water in [Bmmorp][OAc] for CO_2 separation from biogas could decrease the sizes of the absorber and desorber are resulting in a decreased capital cost of absorber and desorber. In addition, the lower amount solvent required using this solvent also led to a decrease in

the size of the solvent pump. As we can see from energy usage in **Fig. 10a**, the compressor contributed 70% of total energy usage, which was related to the pressure of absorption. By decreasing the pressure of absorption from 8 to 7 bar using aqueous [Bmmorp][OAc] with 30 wt.% water (30 wt.%* in **Fig. 10**), the energy usage decrease by 4%, while the diameters of the absorber still 3% smaller than that using PC. These results suggest that using this aqueous [Bmmorp][OAc] has the potential to decrease the energy usage and cost of CO_2 separation from biogas.

4. Conclusions

In this work, the CO_2 absorption capacity in four kinds of aqueous morpholinium based ILs with acetate anions were investigated. Amongst them, [Bmmorp][OAc] is the one with the highest CO_2 absorption capacity, and it was screened for study the effect of water content and temperature on CO_2 absorption capacity and viscosity. The COSMO-based method was used to estimate the thermophysical properties and gas solubility (i.e. CO_2 and CH_4) of the pure IL with high viscosity. The negative enthalpy of solution $\Delta_{sol}H$ was obtained showing the strong intermolecular bonding between the gas (CO_2 and CH_4) and IL.

Combining the determined experimental results and the estimation with COSMO, properties and phase equilibrium were represented with the models embeded in Aspen Plus and process simulation for CO_2 separation from biogas was carried out. The aqueous [Bmmorp][OAc] solutions with 30 to 40 wt.% water in [Bmmorp][OAc] were investigated in this process. The energy usage and the size of equipment of using aqueous [Bmmorp][OAc], water, DEPG, and propylene carbonate for CO_2 separation from biogas were compared. It was found that aqueous [Bmmorp][OAc] had a lower energy usage and smaller size of equipment than the other solvents. The result suggests that using this aqueous [Bmmorp][OAc] can be used as an alternative to commercial organic solvent systems and has the potential to decrease the cost of CO_2 separation. In addition, for the non-volatility of ILs, there is no organic solvent released to the environment and, therefore, this solvent is more environmental-friendly.

Acknowledgments

This work was supported by the Swedish Energy Agency, the Bio4Energy program, the Kempe Foundations and the Swedish Research Council. This work is also a part of the activities of the Johan Gadolin Process Chemistry Centre at Åbo Akademi University as well as the Wallenberg Wood Science Center.

Reference

1. Leung, D. Y. C.; Caramanna, G.; Maroto-Valer, M. M., An overview of current status of carbon dioxide capture and storage technologies. *Renewable and Sustainable Energy Reviews* **2014,** 39, 426-443.
2. Wang, M.; Joel, A. S.; Ramshaw, C.; Eimer, D.; Musa, N. M., Process intensification for post-combustion CO2 capture with chemical absorption: A critical review. *Applied Energy* **2015,** 158, 275-291.
3. Ma, C.; Liu, C.; Lu, X.; Ji, X., Techno-economic analysis and performance comparison of aqueous deep eutectic solvent and other physical absorbents for biogas upgrading. *Applied Energy* **2018,** 225, 437-447.
4. Darde, V.; Thomsen, K.; van Well, W. J. M.; Stenby, E. H., Chilled ammonia process for CO2 capture. *International Journal of Greenhouse Gas Control* **2010,** 4, (2), 131-136.
5. Zeng, S.; Zhang, X.; Bai, L.; Zhang, X.; Wang, H.; Wang, J.; Bao, D.; Li, M.; Liu, X.; Zhang, S., Ionic-Liquid-Based CO2 Capture Systems: Structure, Interaction and Process. *Chemical Reviews* **2017,** 117, (14), 9625-9673.
6. Lei, Z.; Chen, B.; Koo, Y.-M.; MacFarlane, D. R., Introduction: Ionic Liquids. *Chemical Reviews* **2017,** 117, (10), 6633-6635.
7. Raut, D. G.; Sundman, O.; Su, W.; Virtanen, P.; Sugano, Y.; Kordas, K.; Mikkola, J.-P., A morpholinium ionic liquid for cellulose dissolution. *Carbohydrate Polymers* **2015,** 130, 18-25.
8. Galinski, M.; Stepniak, I., Morpholinium-based ionic liquid mixtures as electrolytes in electrochemical double layer capacitors. *Journal of Applied Electrochemistry* **2009,** 39, (10), 1949.
9. Ren, H.-w.; Wang, Q.-h.; Guo, S.-h.; Zhao, D.-s.; Chen, C.-m., The role and potential of morpholinium-based ionic liquids in dissolution of cellulose. *European Polymer Journal* **2017,** 92, 204-212.
10. Xie, Y.; Raut, D. G.; Samikannu, R.; Mikkola, J.-P.; Ji, X., A Thermodynamic Study of Aqueous 1-Allyl-3-Methylimidazolium Formate Ionic Liquid as a Tailored Sorbent for Carbon Dioxide Separation. *Energy Technology* **2017,** 5, (8), 1464-1471.
11. Xie, Y.; Dong, H.; Zhang, S.; Lu, X.; Ji, X., Effect of Water on the Density, Viscosity, and CO_2 Solubility in Choline Chloride/Urea. *Journal of Chemical & Engineering Data* **2014,** 59, (11), 3344-3352.
12. Sarmad, S.; Xie, Y.; Mikkola, J.-P.; Ji, X., Screening of deep eutectic solvents (DESs) as green CO_2 sorbents: from solubility to viscosity. *New Journal of Chemistry* **2017,** 41, (1), 290-301.
13. Tsonopoulos, C., An empirical correlation of second virial coefficients. *AIChE Journal* **1974,** 20, (2), 263-272.
14. Galvão, A. C.; Francesconi, A. Z., Solubility of methane and carbon dioxide in ethylene glycol at pressures up to 14MPa and temperatures ranging from (303 to 423)K. *The Journal of Chemical Thermodynamics* **2010,** 42, (5), 684-688.
15. Valtz, A.; Chapoy, A.; Coquelet, C.; Paricaud, P.; Richon, D., Vapour–liquid equilibria in the carbon dioxide–water system, measurement and modelling from 278.2 to 318.2K. *Fluid Phase Equilibria* **2004,** 226, 333-344.

16. Dalmolin, I.; Skovroinski, E.; Biasi, A.; Corazza, M. L.; Dariva, C.; Oliveira, J. V., Solubility of carbon dioxide in binary and ternary mixtures with ethanol and water. *Fluid Phase Equilibria* **2006,** 245, (2), 193-200.
17. Klamt, A., Conductor-like Screening Model for Real Solvents: A New Approach to the Quantitative Calculation of Solvation Phenomena. *Journal of Physical Chemistry* **1995,** 99, (7), 2224-2235.
18. Klamt, A.; Jonas, V.; Bürger, T.; Lohrenz, J. C. W., Refinement and parameterization of COSMO-RS. *Journal of Physical Chemistry A* **1998,** 102, (26), 5074–5085.
19. Lee, B.-S.; Lin, S.-T., Screening of ionic liquids for CO2 capture using the COSMO-SAC model. *Chemical Engineering Science* **2015,** 121, 157-168.
20. Palomar, J.; Ferro, V. R.; Torrecilla, J. S.; Rodríguez, F., Density and Molar Volume Predictions Using COSMO-RS for Ionic Liquids. An Approach to Solvent Design. *Industrial & Engineering Chemistry Research* **2007,** 46, (18), 6041-6048.
21. Liu, Y.-R.; Thomsen, K.; Nie, Y.; Zhang, S.-J.; Meyer, A. S., Predictive screening of ionic liquids for dissolving cellulose and experimental verification. *Green Chemistry* **2016,** 18, (23), 6246-6254.
22. TURBOMOLE <7.3> <2018>, a development of University of Karlsruhe and Forschungszentrum Karlsruhe GmbH,1989-2007, TURBOMOLE GmbH, since 2007. available from http://www.turbomole.com
23. COSMOtherm <version> (e.g. C3.0, release 1801). http://www.cosmologic.de
24. Eckert, F.; Klamt, A., Fast solvent screening via quantum chemistry: COSMO-RS approach. *AIChE Journal* **2002,** 48, (2), 369-385.
25. Li, X.; Hou, M.; Han, B.; Wang, X.; Zou, L., Solubility of CO_2 in a Choline Chloride + Urea Eutectic Mixture. *Journal of Chemical & Engineering Data* **2008,** 53, (2), 548-550.
26. Valderrama, J. O.; Sanga, W. W.; Lazzús, J. A., Critical Properties, Normal Boiling Temperature, and Acentric Factor of Another 200 Ionic Liquids. *Industrial & Engineering Chemistry Research* **2008,** 47, (4), 1318-1330.
27. Valderrama, J. O.; Robles, P. A., Critical Properties, Normal Boiling Temperatures, and Acentric Factors of Fifty Ionic Liquids. *Industrial & Engineering Chemistry Research* **2007,** 46, (4), 1338-1344.
28. Brelvi, S. W.; O'Connell, J. P., Correspondling states correlations for liquid compressibility and partial molal volumes of gases at infinite dilution in liquids. *AIChE Journal* **1972,** 18, (6), 1239-1243.
29. Zhang, Y.; Que, H.; Chen, C.-C., Thermodynamic modeling for CO2 absorption in aqueous MEA solution with electrolyte NRTL model. *Fluid Phase Equilibria* **2011,** 311, 67-75.
30. Ma, C.; Xie, Y.; Ji, X.; Liu, C.; Lu, X., Modeling, simulation and evaluation of biogas upgrading using aqueous choline chloride/urea. *Applied Energy* **2018,** 229, 1269-1283.

Electronic Supplementary information

CO_2 capture by a series of aqueous morpholinium-based ionic liquids with acetate anions

Chunyan Ma[1,*], Shashi Kant Shukla[2], Rakesh Samikannu[2], Jyri-Pekka Mikkola[2,3], Xiaoyan Ji[1,*]

[1]Division of Energy Science/Energy Engineering, Department of Engineering Science and Mathematics, Luleå University of Technology, Luleå, 971 87, Sweden
[2]Technical Chemistry, Department of Chemistry, Chemical-Biological Centre, Umeå University, Umeå, 90871, Sweden
[3]Industrial Chemistry & Reaction Engineering, Johan Gadolin Process Chemistry Centre, Åbo Akademi University, Biskopsgatan 8, 20500, Finland

1. Characterization

The synthesized ionic liquids were characterized using nuclear magnetic resonance spectroscopy (NMR) Bruker AV 500. ^{1}H and ^{13}C NMR spectra were calibrated using the residual peak of solvents as an internal standard [D_2O (D_2O δH 4.79 ppm, δC no peak)].

The NMR spectral characteristic were shown as below:

Allyl methyl morpholinium acetate [Ammorp][OAc]

^{1}H-NMR (D_2O, 500Hz): - δ (ppm) 1.89 (s, 3H), 3.17 (s, 3H), 3.45 (d, 2H), 3.52 (m, 2H), 4.07 (m, 6H), 5.78 (m, 2H), 6.08 (m, 1H)

^{13}C-NMR (D_2O, 500Hz): - δ (ppm) 180.78, 129.94, 123.33, 67.14, 60.41, 59.09, 46.81, 23.58

Allyl methyl morpholinium acetate [Ammorp][OAc] (after absorbing CO_2)

^{1}H-NMR (D_2O, 500Hz): - δ (ppm) 1.91 (s, 3H), 3.17 (s, 3H), 3.45 (d, 2H), 3.52 (m, 2H), 4.07 (m, 6H), 5.78 (m, 2H), 6.09 (m, 1H)

^{13}C-NMR (D_2O, 500Hz): - δ (ppm) 180.70, 129.94, 123.32, 67.15, 60.42, 59.10, 46.81, 23.46

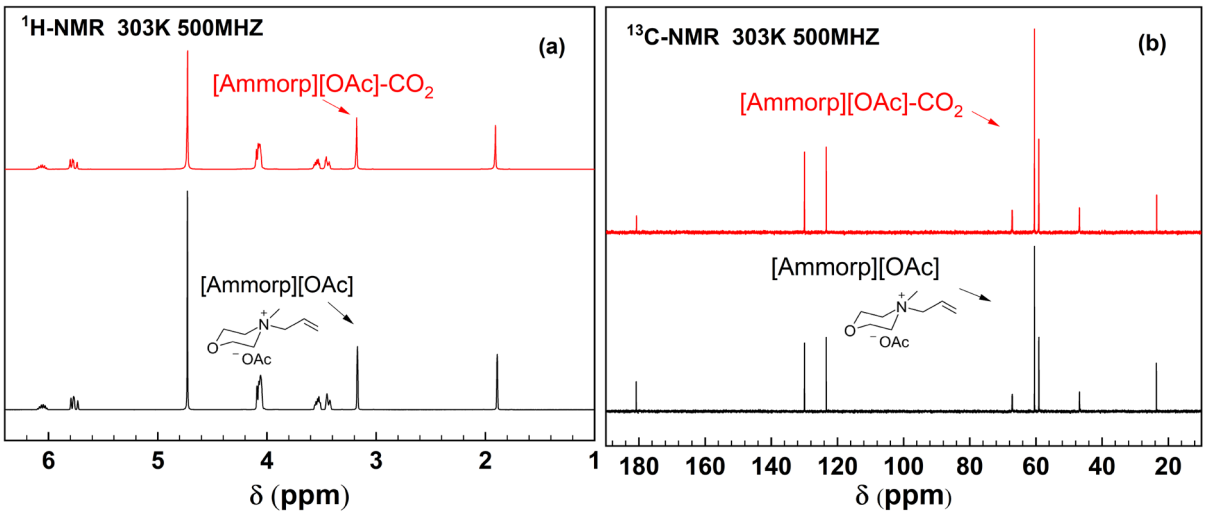

Fig. S1. ^{1}H-(a) and ^{13}C-NMR (b) spectra using D_2O as a solvent for aqueous [Ammorp][OAc] before and after absorbing CO_2

Butyl methyl morpholinium acetate [Bmmorp][OAc]

^{1}H-NMR (D_2O, 500Hz): - δ (ppm) 0.97 (m, 3H), 1.42 (m, 2H), 1.80 (m, 2H), 1.91 (s, 3H), 3.19 (s, 3H), 3.50 (m, 6H), 4.06 (s, 4H)

^{13}C-NMR (D_2O, 500Hz): - δ (ppm) 180.82, 65.18, 60.47, 59.60, 46.83, 23.56, 22.95, 19.16, 12.94

Butyl methyl morpholinium acetate [Bmmorp][OAc] (after absorbing CO_2)

^{1}H-NMR (D_2O, 500Hz): - δ (ppm) 0.97 (m, 3H), 1.42 (m, 2H), 1.80 (m, 2H), 1.91 (s, 3H), 3.19 (s, 3H), 3.50 (m, 6H), 4.05 (s, 4H)

^{13}C-NMR (D_2O, 500Hz): - δ (ppm) 180.72, 65.18, 60.47, 59.60, 46.84, 23.44, 22.95, 19.16, 12.92

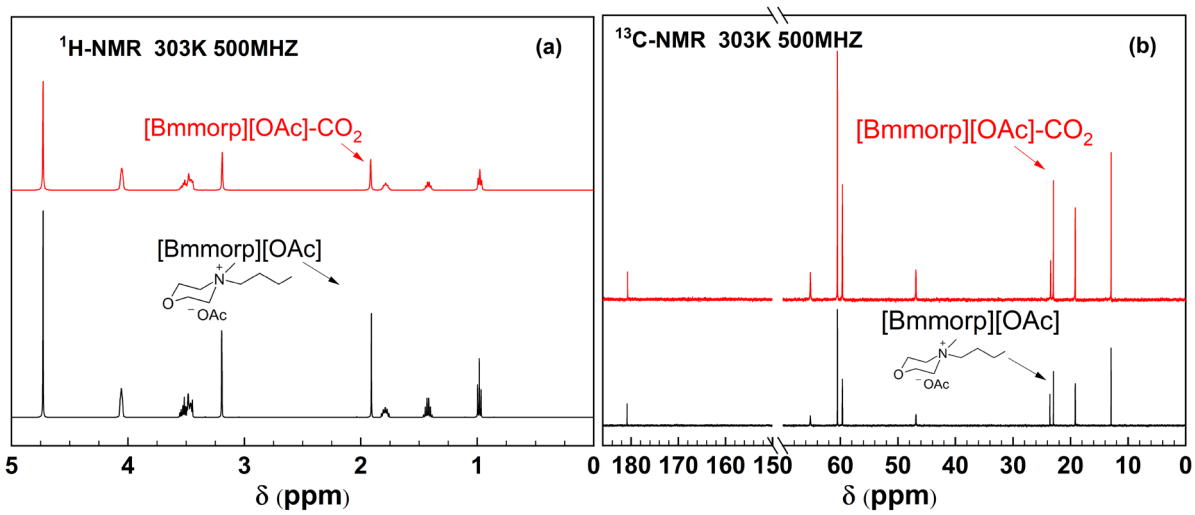

Fig. S2. ^{1}H-(a) and ^{13}C-NMR (b) spectra using D_2O as a solvent for aqueous [Bmmorp][OAc] before and after absorbing CO_2

Ethyl methyl morpholinium acetate [Emmorp][OAc]

^{1}H-NMR (D_2O, 500Hz): - δ (ppm) 1.38 (m, 3H), 1.92 (s, 3H), 3.18 (s, 3H), 3.50 (m, 4H), 3.58 (m, 2H), 4.06 (s, 4H)

^{13}C-NMR (D_2O, 500Hz): - δ (ppm) 180.90, 60.87, 60.47, 59.17, 46.16, 23.53, 6.64

Ethyl methyl morpholinium acetate [Emmorp][OAc] (after absorbing CO_2)

^{1}H-NMR (D_2O, 500Hz): - δ (ppm) 1.38 (m, 3H), 1.91 (s, 3H), 3.17 (s, 3H), 3.47 (m, 4H), 3.53 (m, 2H), 4.06 (s, 4H)

^{13}C-NMR (D_2O, 500Hz): - δ (ppm) 180.73, 60.88, 60.48, 59.15, 46.17, 23.50, 6.66

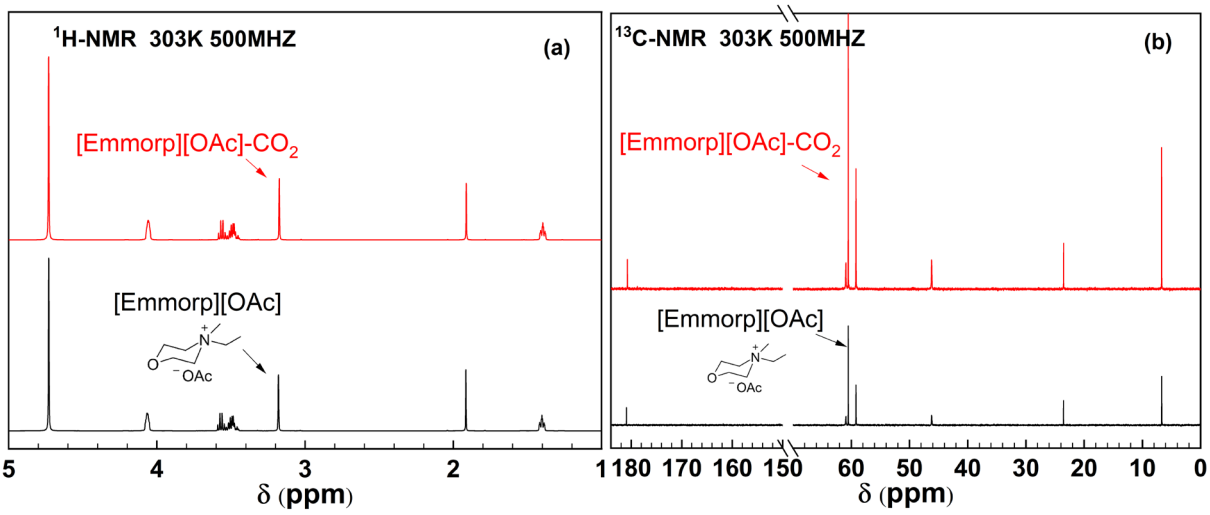

Fig. S3. ^{1}H-(a) and ^{13}C-NMR (b) spectra using D_2O as a solvent for aqueous [Emmorp][OAc] before and after absorbing CO_2

Propyl methyl morpholinium acetate [Pmmorp][OAc]

^{1}H-NMR (D_2O, 500Hz): - δ (ppm) 1.0 (m, 3H), 1.81 (m, 2H), 1.84 (m, 2H), 1.91 (s, 3H), 3.19 (s, 3H), 3.48 (m, 6H), 4.05 (s, 4H)

^{13}C-NMR (D_2O, 500Hz): - δ (ppm) 180.89, 66.64, 60.45, 59.60, 46.89, 23.52, 14.74, 9.96

Propyl methyl morpholinium acetate [Pmmorp][OAc] (after absorbing CO_2)

^{1}H-NMR (D_2O, 500Hz): - δ (ppm) 1.0 (m, 3H), 1.81 (m, 2H), 1.84 (m, 2H), 1.91 (s, 3H), 3.19 (s, 3H), 3.47 (m, 6H), 4.05 (s, 4H)

^{13}C-NMR (D_2O, 500Hz): - δ (ppm) 180.80, 66.65, 60.46, 59.60, 46.89, 23.45, 14.75, 9.96

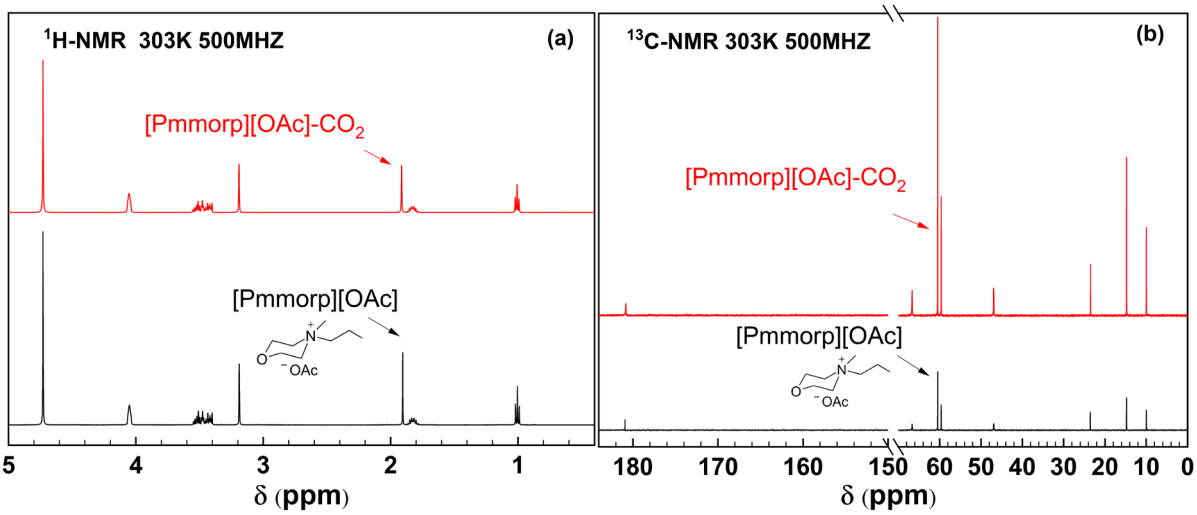

Fig. S4. ^{1}H-(a) and ^{13}C-NMR (b) spectra using D_2O as a solvent for aqueous [Pmmorp][OAc] before and after absorbing CO_2

2. The validation of gas solubility by our experimental method

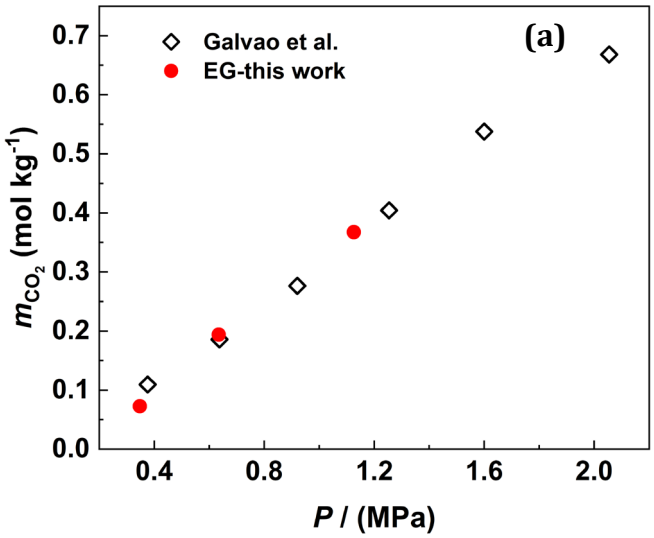

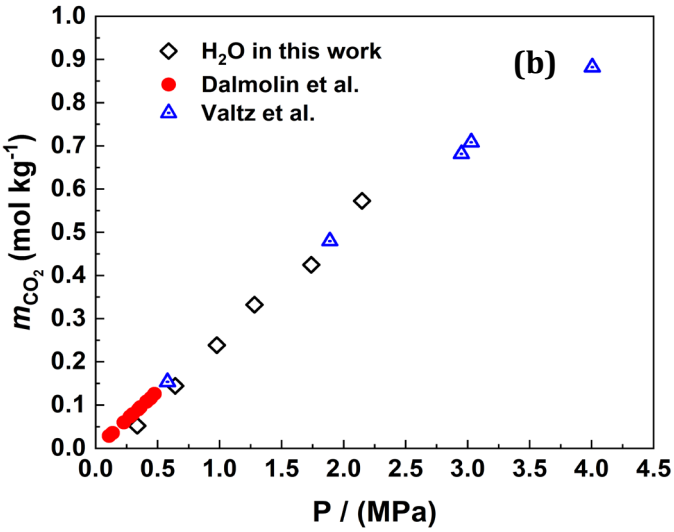

Fig. S5 Solubilities of CO_2 in (a) ethylene glycol and (b) H_2O

3. Thermophysical properties estimated by COSMOthermX

Table S1 Thermophysical properties for [Bmmorp][OAc] estimated by COSMOthermX

T / (K)	Density ρ / (g cm^{-3})	Viscosity η / (mPa s)	Electrical conductivity Λ / (mS cm^{-1})	Heat capacity C_p / (J mol^{-1} K^{-1})
298.15	1.036	473.698	0.561	398.454
308.15	1.029	263.980	0.949	
318.15	1.023	155.934	1.510	
323.15	1.020	122.213	1.866	418.467
328.15	1.017	96.934	2.278	
338.15	1.011	63.023	3.285	